Color-stable, ITO-free white organic light-emitting diodes with enhanced efficiency using solution-processed transparent electrodes and optical outcoupling layers

Hong-Wei Chang[1,2 †], Yong Hyun Kim[1 †], Jonghee Lee[1,3], Simone Hofmann[1], Björn Lüssem[1], Lars Müller-Meskamp[1], Malte C. Gather[1,4], Karl Leo[1]*[a], and Chung-Chih Wu[2]*[b]

[1] *Institut für Angewandte Photophysik, George-Bähr-Strasse 1, 01062 Dresden, Germany*

[2] *Graduate Institute of Electronics Engineering, Graduate Institute of Photonics and Optoelectronics, and Department of Electrical Engineering, National Taiwan University, Taipei 106, Taiwan*

[3] *OLED Research Team, Electronics and Telecommunications Research Institute (ETRI), Daejeon 305-700, South Korea*

[4] *SUPA, School of Physics and Astronomy, University of St Andrews, St Andrews, KY16 9SS, UK*

† Authors contributed equally in this work

***[a] e-mail: karl.leo@iapp.de**

***[b] e-mail: chungwu@cc.ee.ntu.edu.tw**

Abstract

In this work, we demonstrate color-stable, ITO-free white organic light-emitting diodes (WOLEDs) with enhanced efficiencies by combining the high-conductivity conducting polymer PEDOT:PSS as transparent electrode and a nanoparticle-based scattering layer (NPSL) as the effective optical out-coupling layer. In addition to efficiency enhancement, the NPSL is also beneficial to the stabilization of electroluminescent spectra/colors over viewing angles. Both the PEDOT:PSS and the NPSL can be fabricated by simple, low-temperature solution processing. The integration of both solution-processable transparent electrodes and light extraction structures into OLEDs is particularly attractive for applications since they simultaneously provide manufacturing, cost and efficiency advantages.

Keywords: OLEDs; transparent electrode; conducting polymer; optical outcoupling;

1. Introduction

Organic light emitting diodes (OLEDs) are typically realized with a transparent indium tin oxide (ITO) anode, which is brittle, expensive, thus limiting the low-cost manufacturing and mechanical flexibility of OLEDs. ITO electrodes generally require a high-temperature processing for crystallization of films, which also limits the use of flexible substrates. Furthermore, the energy level mismatch between the work function of ITO and the highest occupied molecular orbital (HOMO) of typical organic hole transport layers often hinders hole injection and formation of ohmic contacts.[1-5] Accordingly, alternative transparent electrodes for the replacement of ITO, such as carbon nanotubes,[6] graphene,[7] thin metals,[8, 9] metal grids,[10] metal nanowires [11] and conducting polymers [12-14] have been widely investigated. Among them, the conducting polymer poly(3,4-ethylenedioxythiophene):poly(styrenesulfonate) (PEDOT:PSS) has attracted particular attention due to its excellent mechanical flexibility, chemical stability, good transmittance and conductivity, and low cost.[15] Various methods to improve the performance of PEDOT:PSS (particularly the conductivity) have been recently reported and these electrodes have been successfully used as transparent electrodes for OLEDs [16, 17] as well as organic solar cells.[18]

Similar to other solid-state lighting sources, typical OLEDs also suffer from a poor extraction efficiency of internally generated photons, resulting from a large mismatch of the refractive index between organic layers (n~1.7-1.9), ITO (n~1.8-2.0), glass (n~1.5), and air (n~1.0). The total internal reflection at the interfaces of devices strongly traps photons inside the device, which significantly limits the external quantum efficiency (EQE) of OLEDs. It is known that ~70-80% of the generated photons are trapped in conventional OLED structures due to total internal reflection or coupling to localized surface plasmon polaritons (SPPs) at the metallic surface, [19-21]

while internal quantum efficiencies of fully phosphorescent [22] and triplet-harvesting OLEDs [23] close to 100% have been reported. In order to overcome the limited optical outcoupling efficiency of OLEDs, various strategies of using internal or external light extraction layers/structures have been investigated.[24-28] External light extraction structures are typically constructed outside of the device (i.e. on the substrate side having no OLED devices). For instance, OLEDs can be combined with micro-lens arrays [24] or shaped substrates to extract the substrate modes.[25]

Internal light extraction structures are typically fabricated between organic layers and substrates, which ideally provides access to efficient light extraction for both organic and substrate modes and thus should in principle yield higher extraction efficiencies than external extraction methods. Photonic crystals [26] and embedded low index grids [24] have been investigated as effective internal light extraction structures for OLEDs. However, these internal extraction architectures in general involve more complicated fabrication and thus are not cost-effective for real OLED applications. Recently, we have developed nanoparticle-based scattering layers (NPSLs) as effective internal extraction structures for OLEDs [29-31]. The strong light scattering effect prevents total internal reflection at internal interfaces, enabling extraction of more photons from devices. Such NPSLs can be readily prepared by mixing nanoparticles with polymer hosts and be coated by solution casting, which results in possessing cost and manufacturing advantages. In addition to enhancing optical out-coupling efficiencies of OLEDs, one also generally finds that the color stability of OLEDs over viewing angles is improved when NPSLs are incorporated, an effect we have attributed to re-mixing of emission over angles.[29-31]

Here, by combining the high-conductivity polymer PEDOT:PSS as the transparent electrode and NPSLs as an effective optical out-coupling layer, we demonstrate color-stable, ITO-free white OLEDs (WOLEDs) with enhanced efficiency. Both the

PEDOT:PSS and the NPSL can be fabricated by a simple, low-temperature solution processing method, making such structures and methods particularly attractive for applications.

2. Methods

2.1. Preparation and characterization of PEDOT:PSS electrodes

Thin films of high-conductivity PEDOT:PSS were prepared by spin-coating from a mixture solution of the aqueous PEDOT:PSS solution (Clevios PH1000, Heraeus) and 6 vol.% ethylene glycol (EG). Adding the co-solvent EG into the PEDOT:PSS has been reported to substantially increase the conductivity of PEDOT:PSS.[18] Spin-coated PEDOT:PSS films were subsequently annealed on a hot plate at 120 °C for 15 minutes under ambient conditions. The sheet resistance of the films was measured by the Van der Pauw method. The thicknesses of the PEDOT:PSS electrodes were measured by a surface profilometer (Veeco Dektak 150). The transmittance of PEDOT:PSS thin films was measured using a spectrophotometer (Shimadzu MPC 3100). The PEDOT:PSS films were laterally structured by laser ablation with a Nd:YAG laser (ACI Laser) for the use as bottom electrodes in OLEDs.

2.2. Preparation and characterization of NPSL

For preparation of the NPSL mixture solution, 600 mg of TiO_2 nanoparticles was added into a 4cc solution of the organic host material. TiO_2 nanoparticles with an average diameter of ~240 nm were dispersed homogeneously in a solution of an organic host matrix by physical vibration/stirring in the presence of ~100 μm diameter ZrO_2 particles as a milling object. The nanoparticle size was chosen to give strong enough optical scattering and yet not to induce significant surface roughnesses of films. The host matrix consisted of a propylene glycol-monomethyl-ether

acetate-based and methyl-isopropyl ketone-based transparent photoresist material (Everlight Chemical Industrial Corporation). The NPSL films were then prepared through spin-coating of the filtered mixture solution of photoresist/TiO_2 nanoparticles at 1000 rpm for 40 seconds, followed by heat curing at 130 °C for 10 minutes. The morphology of NPSL was analyzed by atomic force microscopy (AFM) and scanning electron microscopy (SEM), and the average root-mean-square (RMS) roughness of the films was determined by analyzing a scanning area of 5x5 μm^2.

A UV-Vis spectrophotometer equipped with an integrating sphere (JASCO V570) was used to characterize the transmittance and optical scattering properties of the NPSL films. In this work, two different transmittance measures are used. The specular transmittance ($T_{specular}$), representing photons transmitted parallel to the incident beam, was measured by using a monochromatic light beam incident normal on the sample and then collecting transmitted light only in the normal direction (within a 5° collection angle). The total transmittance (T_{total}), representing both scattered or non-scattered photons, was measured by using a monochromatic light beam incident normal on sample and then using an integrating sphere to collect transmitted light over all angles. The diffuse transmittance ($T_{diffuse}$), representing photons scattered into all but the incident directions, could then be calculated as $T_{diffuse} = T_{total} - T_{specular}$. The *haze*, which is defined as the ratio of the diffusively transmitted light over the total transmitted light, was then calculated as $haze = T_{diffuse}/T_{total}$.

2.3. Fabrication and characterization of OLEDs

Four types of WOLEDs are investigated in this study, including an reference ITO-based device (*ITO device*), a reference PEDOT:PSS-based device (*PEDOT device*), a *PEDOT device* with an external NPSL, and a *PEDOT device* with an internal NPSL (see **Figure 1**). All devices were fabricated by thermal evaporation in a

vacuum chamber (K. J. Lesker) with a base pressure of $<10^{-7}$ mbar. These devices were encapsulated using an additional cover glass and epoxy resin in nitrogen atmosphere and were measured under ambient conditions. The WOLED stack (**Figure 2**) in general had a tandem structure of two emitting units, one (top unit) containing a p-i-n phosphorescent green/yellow double-emitting-layer structure and the other (bottom unit) containing a p-i-n fluorescent (blue)/phosphorescent (red) hybrid triplet-harvesting emitting structure.[23] The overall stack consisted of: glass/ ITO (90 nm), PEDOT:PSS (90 nm), or PEDOT:PSS with NPSL/ MeO-TPD:F6TCNNQ (2wt. %, 35 nm)/ Spiro-TAD (10 nm)/ 4P-NPD: $Ir(MDQ)_2(acac)$ (5wt. %, 5 nm)/ 4P-NPD (5 nm)/ BPhen (10 nm)/ BPhen: Cs (90 nm)/ Ag (0.5 nm)/ MeO-TPD: F6TCNNQ (2wt. %, 75 nm)/ Spiro-TAD (10 nm)/ TCTA: $Ir(ppy)_3$:$Ir(dhfpy)_2(acac)$ (91 wt. %: 8wt. %: 1wt. %, 5 nm)/ TPBI: $Ir(ppy)_3$:$Ir(dhfpy)_2(acac)$ (91 wt. %: 8wt. %: 1wt. %, 5 nm)/ TPBI (10 nm)/ BPhen: Cs (60 nm)/ Al (100 nm). MeO-TPD (N,N,N',N'-tetrakis(4-methoxyphenyl)-benzidine, Sensient) doped with F6TCNNQ (2,2'-(perfluoronaphthalene-2,6-diylidene) dimalononitrile, Novaled) was used as a p-doped hole injection and transport layer. Spiro-TAD (2,2',7,7'-tetrakis(N,N-diphenylamino)-9,90-spirobifluorene, Lumtec) served as a hole-transport and electron/exciton blocking layer. 4P-NPD (N,N'-di-1-naphthalenyl-N,N0-diphenyl-[1,1':4',1'':4'',1'''-quaterphenyl]-4,4'''-diam ine, Lumtec) doped with $Ir(MDQ)_2(acac)$ (bis(2-methyldibenzo-[f,h] quinoxaline) (acetylacetonate) iridium(III), Lumtec) was the phosphorescent red emitting layer. 4P-NPD served as a fluorescent blue emitting layer. BPhen (4,7-diphenyl-1,1'-phenanthroline, ABCR) or TPBi (2,2',2''-1,3,5-(benzenetriyl)-tris[1-phenyl-1 H-benzimidazole], Sensient) served as the electron-transport and hole/exciton blocking layer. BPhen doped with Cs was an n-doped electron injection and transport layer. Thin Ag (0.5 nm) served as a charge

generation layer of the tandem structure. TCTA (4,4',4''-tris(N-carbazolyl)-triphenylamine, Sensient) and TPBI simultaneously doped with $Ir(ppy)_3$ (fac-tris(2-phenylpyridine) iridium (III), Lumtec) and $Ir(dhfpy)_2(acac)$ (bis(2 -(9,9-dihexylfluorenyl)-1-pyridine) (acetylacetonate) iridium(III), Lumtec) as phosphorescent green/yellow emitting layers.[23] Al (100 nm) was the cathode. The active area of all devices was 6.49 mm^2 as defined by the in-situ shadow masking.

A silicon photodiode and a source-measurement unit SMU 2400 (Keithley) were used for the measurement of the luminance and current-voltage characteristics of OLEDs. The silicon photodiode was calibrated with a spectrometer CAS140CT-153 from the Instrument Systems GmbH for the absolute intensity. The angle-dependent measurements were carried out on a goniometer setup with a USB-4000 mini-spectrometer (Ocean Optics, Inc.).

3. Results and Discussion

3.1. Characteristics of PEDOT:PSS electrodes

When adding the 6 vol.% EG co-solvent into the PEDOT:PSS aqueous solution, the spin-coated PEDOT:PSS film (90 nm thick) achieved a sheet resistance of ~150 ohm/□ and a conductivity of 740 S cm^{-1}, rendering it orders of magnitude more conductive than PEDOT:PSS films coated from original aqueous solutions. Such high-conductivity PEDOT:PSS films provide sufficient conductivity for use as the transparent electrode in OLEDs. According to previous studies, the enhanced conductivity of PEDOT:PSS could be attributed to a strong phase separation of conducting PEDOT and insulating PSS domains by the addition of EG, leading to the formation of more organized conducting pathways of PEDOT and thus much more efficient charge conduction.[17] **Figure 3** shows the specular transmittance ($T_{specular}$)

spectrum of the high-conductivity PEDOT:PSS, compared to that of a conventional ITO electrode (also 90 nm thick). It shows that the high-conductivity PEDOT:PSS electrode exhibits a transmittance (e.g., 88% at 520 nm) similar to or even higher than that of ITO throughout the visible range (400-700 nm).

3.2. Characteristics of NPSL

Rather smooth and uniform NPSL films were obtained by the methods described in the previous section. More details on characterization and properties of the NPSL indeed had been discussed in our previous reports [29-31]. The thickness of the NPSL film was ~2 μm. The spectra of $T_{specular}$ and T_{total} for the NPSL film are shown in **Figure 4**. In **Figure 4**, one sees that the NPSL exhibits a low $T_{specular}$ over most of the visible region and yet a high T_{total} of 40-70%, corresponding to a high *haze* of 95-50% (haze is defined in sect. 2.2) and indicating effective light scattering induced by the NPSL over the entire visible wavelength range. In consideration of the high transparency and low *haze* (<3%) of the pure host film and the large difference in refractive indices of the host material (1.52 at 520 nm) and TiO_2 (2.2 at 520 nm), these results indicate that the strong optical scattering of the NPSL mainly originates from added nanoparticles. The average RMS surface roughness of the NPSL (as determined by AFM) was around 3.6 nm, which is in the acceptable range for subsequent device integration. The NPSL had a sufficiently strong adhesion to the substrate surface and could endure subsequent device processing steps, such as the coating of the PEDOT:PSS layers and deposition of other OLED layers on top of it.

3.3. Characteristics of WOLEDs

Figure 5 shows J-V-L characteristics (**5a**), external quantum efficiency (EQE) (**5b**), and power efficiency (PE) (**5c**) for all devices: the ITO device, the PEDOT device, the

PEDOT device with an external NPSL, and the PEDOT device with an internal NPSL. Electroluminescent characteristics of these OLEDs are also summarized in **Table 1**. The PEDOT device exhibits an EQE (~13% at 1000 cd/m^2) similar to that of the ITO reference device (~14% at 1000 cd/m^2), although the operating voltage required in the PEDOT device to reach a given current density is slightly higher than in the ITO device. The slightly higher operating voltage of the PEDOT device may be associated with its higher sheet resistance (vs. ITO). Nevertheless, one sees that the high-conductivity PEDOT:PSS can be successfully used as a single transparent electrode/anode of an OLEDs. In **Figure 5a**, one also sees that the PEDOT devices with and without internal or external NPSL show similar electrical characteristics (J-V characteristics), indicating that even when the NPSL is inserted as an internal optical extraction structure between the substrate and the PEDOT:PSS the electrical characteristics are not degraded (e.g., device shorting or serious leakage current etc.).

With similar J-V characteristics for all PEDOT:PSS based OLEDs, the modification of the optical characteristics (efficiency, color, viewing angle characteristics etc.) can be mainly attributed to NPSL-induced optical effects. For devices with the NPSL integrated inside the OLED (i.e., the PEDOT device with internal NPSL), the external quantum efficiency was improved from 12.82% (at 1000 cd/m^2) of the PEDOT device to 17.24% (at 1000 cd/m^2), corresponding to an enhancement by 1.34 times. The power efficiency was correspondingly enhanced as well. On the other hand, with coating the NPSL to the outside of the device (i.e., the PEDOT device with external NPSL), the external quantum efficiency was only slightly enhanced by a factor less than 1.1. This indicates that the internal NPSL is substantially more effective in light extraction than the external NPSL, presumably because an internal NPSL can affect both the organic and substrate modes of the device while the external NPSL can only access the latter. Although the efficiency enhancement achieved here is modest, the

current work successfully demonstrates integration of both solution-processable transparent electrodes and light extraction structures into OLEDs. The combination of these two concepts may simultaneously provide manufacturing, cost and efficiency advantages. In the future, by optimizing the OLED structure and the NPSL, larger enhancement may be expected.

Figure 6 shows the EL spectra with respect to the viewing angle for all four devices. In both the *ITO device* (**Figure 6a**) and the *PEDOT device* (**Figure 6b**), one observes that EL spectra (and thus the color) vary significantly with viewing angles. This is also seen as a substantial variation of the $CIE_{x,y}$ (Comission Internationle de l'Eclairage) coordinates of these two devices with viewing angle. As illustrated in **Figure 7a** and **Figure 7b**, for both devices, the shift of CIE_x and CIE_y coordinates with viewing angle is larger than 0.02 (**Table 1**). By contrast, incorporating the NPSL into the device (either externally or internally) strongly reduce the change of the EL spectra (and thus the color) with viewing angle (PEDOT device with external NPSL, **Figure 6c** and the PEDOT device with internal NPSL, **Figure 6d**). Correspondingly, the shifts of CIE_x and CIE_y coordinates over viewing angles are significantly suppressed (<0.003, **Figure 7c**, **Figure 7d**, **Table 1**). These results indicate that in addition to enhancing the optical out-coupling efficiency of OLEDs, the NPSL is also beneficial for the stabilization of EL spectra/colors over viewing angles.

In addition to the emission properties of the emitting materials themselves, the EL spectra/colors and their viewing-angle dependence in typical OLED structures in general is also strongly associated with the optical microcavity/interference effects (and thus the optical structures and optical properties of material layers) in the devices. As an instance, since ITO and PEDOT anodes possess very different refractive indices (n~1.9 for ITO, n~1.48 for PEDOT), the *ITO device* and the *PEDOT device* show different EL spectra/colors even they have same organic layer stacks. With NPSL

films incorporated, on one hand, optical scattering could induce re-mixing/averaging of emission of different angles. On the other hand, optical scattering by the NPSL would also strongly perturb the phases and propagation directions of the lightwaves, and thus also the microcavity and interference effects in OLEDs. These perhaps together contribute to the significant improvements in color stability over viewing angles.

4. Conclusions

In summary, by combining the high-conductivity polymer PEDOT:PSS as the transparent electrode with nanoparticle-based scattering layers, we demonstrated color-stable, ITO-free white OLEDs (WOLEDs) with enhanced out-coupling efficiencies. In addition to the efficiency enhancement, the NPSL also stabilizes the EL spectra and emission color over viewing angles. Both the PEDOT:PSS and the NPSL can be fabricated by simple, low-temperature solution processes. Integration of both solution-processable transparent electrodes and light extraction structures for OLEDs is particularly attractive for applications since they may simultaneously provide manufacturing, cost and efficiency advantages.

Acknowledgements:

This work was supported by the German BMBF (13N11060, project R2FLEX) and the National Science Council and Ministry of Education of Republic of China (Taiwan) (NSC-99-2221-E-002-118-MY3 and 10R70607). H.-W. Chang acknowledges financial support as fellow of Deutscher Akademischer Austauschdienst (DAAD). J. Lee acknowledges the Alexander von Humboldt Foundation and the IT R&D program of MKE/KEIT (Grant No. 10041416, the core technology development of light- and space-adaptable new mode display for energy

savings at 7 inches and 2 W).

References:

[1] L. Chkoda, C. Heske, M. Sokolowski, E. Umbach, F. Steuber, J. Staudigel, M. Stößel, J. Simmerer, Work function of ITO substrates and band-offsets at the TPD/ITO interface determined by photoelectron spectroscopy, Synthetic Metals, 111–112 (2000) 315-319.

[2] D.J. Milliron, I.G. Hill, C. Shen, A. Kahn, J. Schwartz, Surface oxidation activates indium tin oxide for hole injection, Journal of Applied Physics, 87 (2000) 572-576.

[3] J.C. Scott, J.H. Kaufman, P.J. Brock, R. DiPietro, J. Salem, J.A. Goitia, Degradation and failure of MEH-PPV light-emitting diodes, Journal of Applied Physics, 79 (1996) 2745-2751.

[4] J.M. Phillips, J. Kwo, G.A. Thomas, S.A. Carter, R.J. Cava, S.Y. Hou, J.J. Krajewski, J.H. Marshall, W.F. Peck, D.H. Rapkine, R.B. van Dover, Transparent conducting thin films of GaInO[sub 3], Applied Physics Letters, 65 (1994) 115-117.

[5] Y. Park, V. Choong, Y. Gao, B.R. Hsieh, C.W. Tang, Work function of indium tin oxide transparent conductor measured by photoelectron spectroscopy, Applied Physics Letters, 68 (1996) 2699-2701.

[6] M.W. Rowell, M.A. Topinka, M.D. McGehee, H.-J. Prall, G. Dennler, N.S. Sariciftci, L. Hu, G. Gruner, Organic solar cells with carbon nanotube network electrodes, Applied Physics Letters, 88 (2006) 233506-233503.

[7] L. Gomez De Arco, Y. Zhang, C.W. Schlenker, K. Ryu, M.E. Thompson, C. Zhou, Continuous, Highly Flexible, and Transparent Graphene Films by Chemical Vapor Deposition for Organic Photovoltaics, ACS Nano, 4 (2010) 2865-2873.

[8] J. Meiss, M.K. Riede, K. Leo, Towards efficient tin-doped indium oxide (ITO)-free inverted organic solar cells using metal cathodes, Applied Physics Letters, 94 (2009) 013303-013303.

[9] T. Schwab, S. Schubert, L. Müller-Meskamp, K. Leo, M.C. Gather, Eliminating Micro-Cavity Effects in White Top-Emitting OLEDs by Ultra-Thin Metallic Top Electrodes, Advanced Optical Materials, (2013) n/a-n/a, DOI: 10.1002/adom.201300392.

[10] M.-G. Kang, M.-S. Kim, J. Kim, L.J. Guo, Organic Solar Cells Using Nanoimprinted Transparent Metal Electrodes, Advanced Materials, 20 (2008) 4408-4413.

[11] W. Gaynor, S. Hofmann, M.G. Christoforo, C. Sachse, S. Mehra, A. Salleo, M.D. McGehee, M.C. Gather, B. Lüssem, L. Müller-Meskamp, P. Peumans, K. Leo, Color in the Corners: ITO-Free White OLEDs with Angular Color Stability, Advanced Materials, 25 (2013) 4006-4013.

[12] S.-I. Na, S.-S. Kim, J. Jo, D.-Y. Kim, Efficient and Flexible ITO-Free Organic Solar Cells Using Highly Conductive Polymer Anodes, Advanced Materials, 20 (2008)

4061-4067.
[13] F. Zhang, M. Johansson, M.R. Andersson, J.C. Hummelen, O. Inganäs, Polymer Photovoltaic Cells with Conducting Polymer Anodes, Advanced Materials, 14 (2002) 662-665.
[14] Y. Zhou, F. Zhang, K. Tvingstedt, S. Barrau, F. Li, W. Tian, O. Inganas, Investigation on polymer anode design for flexible polymer solar cells, Applied Physics Letters, 92 (2008) 233308-233303.
[15] J. Cui, A. Wang, N.L. Edleman, J. Ni, P. Lee, N.R. Armstrong, T.J. Marks, Indium Tin Oxide Alternatives—High Work Function Transparent Conducting Oxides as Anodes for Organic Light-Emitting Diodes, Advanced Materials, 13 (2001) 1476-1480.
[16] Y.H. Kim, J. Lee, S. Hofmann, M.C. Gather, L. Müller-Meskamp, K. Leo, Achieving High Efficiency and Improved Stability in ITO-Free Transparent Organic Light-Emitting Diodes with Conductive Polymer Electrodes, Advanced Functional Materials, 23 (2013) 3763-3769.
[17] K. Fehse, K. Walzer, K. Leo, W. Lövenich, A. Elschner, Highly Conductive Polymer Anodes as Replacements for Inorganic Materials in High-Efficiency Organic Light-Emitting Diodes, Advanced Materials, 19 (2007) 441-444.
[18] Y.H. Kim, C. Sachse, M.L. Machala, C. May, L. Müller-Meskamp, K. Leo, Highly Conductive PEDOT:PSS Electrode with Optimized Solvent and Thermal Post-Treatment for ITO-Free Organic Solar Cells, Advanced Functional Materials, 21 (2011) 1076-1081.
[19] V. Bulović, V.B. Khalfin, G. Gu, P.E. Burrows, D.Z. Garbuzov, S.R. Forrest, Weak microcavity effects in organic light-emitting devices, Physical Review B, 58 (1998) 3730-3740.
[20] C.-L. Lin, T.-Y. Cho, C.-H. Chang, C.-C. Wu, Enhancing light outcoupling of organic light-emitting devices by locating emitters around the second antinode of the reflective metal electrode, Applied Physics Letters, 88 (2006) 081114-081114-081113.
[21] K. Neyts, Microcavity effects and the outcoupling of light in displays and lighting applications based on thin emitting films, Applied surface science, 244 (2005) 517-523.
[22] Y. Kawamura, K. Goushi, J. Brooks, J.J. Brown, H. Sasabe, C. Adachi, 100% phosphorescence quantum efficiency of Ir(III) complexes in organic semiconductor films, Applied Physics Letters, 86 (2005) 071104-071103.
[23] T.C. Rosenow, M. Furno, S. Reineke, S. Olthof, B. Lussem, K. Leo, Highly efficient white organic light-emitting diodes based on fluorescent blue emitters, Journal of Applied Physics, 108 (2010) 113113-113113-113115.
[24] Y. Sun, S.R. Forrest, Enhanced light out-coupling of organic light-emitting devices

using embedded low-index grids, Nature Photonics, 2 (2008) 483-487.
[25] Y. Sun, S.R. Forrest, Organic light emitting devices with enhanced outcoupling via microlenses fabricated by imprint lithography, Journal of Applied Physics, 100 (2006) 073106-073106-073106.
[26] Y.R. Do, Y.C. Kim, Y.W. Song, C.O. Cho, H. Jeon, Y.J. Lee, S.H. Kim, Y.H. Lee, Enhanced Light Extraction from Organic Light-Emitting Diodes with 2D SiO2/SiNx Photonic Crystals, Advanced Materials, 15 (2003) 1214-1218.
[27] T.-H. Han, Y. Lee, M.-R. Choi, S.-H. Woo, S.-H. Bae, B.H. Hong, J.-H. Ahn, T.-W. Lee, Extremely efficient flexible organic light-emitting diodes with modified graphene anode, Nat Photon, 6 (2012) 105-110.
[28] S. Reineke, F. Lindner, G. Schwartz, N. Seidler, K. Walzer, B. Lussem, K. Leo, White organic light-emitting diodes with fluorescent tube efficiency, Nature, 459 (2009) 234-238.
[29] H.-W. Chang, J. Lee, S. Hofmann, Y.H. Kim, L. Muller-Meskamp, B. Lussem, C.-C. Wu, K. Leo, M.C. Gather, Nano-particle based scattering layers for optical efficiency enhancement of organic light-emitting diodes and organic solar cells, Journal of Applied Physics, 113 (2013) 204502-204508.
[30] H.-W. Chang, J. Lee, T.-W. Koh, S. Hofmann, B. Lüssem, S. Yoo, C.-C. Wu, K. Leo, M.C. Gather, Bi-directional organic light-emitting diodes with nanoparticle-enhanced light outcoupling, Laser & Photonics Reviews, 7 (2013) 1079-1087.
[31] Ho.-W. Chang, K.-C. Tien, M.-H. Hsu, Y.-H. Huang, M.-S. Lin, C.-H. Tsai, Y.-T. Tsai , C.-C. Wu, Organic Light Emitting Devices Integrated with Internal Scattering Layers for Enhancing Optical Out-Coupling, Journal of the Society for Information Display, 19 (2011) 196-204.

Table and Figure Captions

Table 1. Summary of EL characteristics of all four OLEDs investigated in this study. EQE is external quantum efficiency, PE is power efficiency, EQEx is the EQE enhancement factor (vs. the PEDOT reference device without outcoupling enhancement), max. ΔCIE_x and max. ΔCIE_y are the maximal shifts of CIE_x and CIE_y color coordinates (relative to those at 0°) over different viewing angles.

Figure 1. Schematic device structures of **a**, the *ITO device*. **b**, the *PEDOT device*. **c**, the *PEDOT device* with external NPSL. **d**, the *PEDOT device* with internal NPSL.

Figure 2. Schematic of the OLED layer stack used in this work.

Figure 3. Transmittance spectra of ITO (black square ■) and PEDOT:PSS thin films (red circle ○).

Figure 4. Spectra of total transmittance ($T_{total,}$ black line) and specular transmittance ($T_{specular,}$ black dash) of NPSL.

Figure 5. OLED characteristics: **a**, current density-voltage-luminance (J-V-L) characteristics. **b**, external quantum efficiency (EQE, %) as a function of luminance. **c**, power efficiency (lm W^{-1}) as a function of luminance.

Figure 6. EL Spectra of OLEDs devices at different viewing angles from 0° to 60°, for **a**, the *ITO device*. **b**, the *PEDOT device*. **c**, the *PEDOT device* with external NPSL. **d**, the *PEDOT device* with internal NPSL.

Figure 7. $CIE_{x,y}$1931 color coordinates of OLED EL over viewing angles from 0° to 60° for **a**, the *ITO device*. **b**, the *PEDOT device*. **c**, the *PEDOT device* with external NPSL. **d**, the *PEDOT device* with internal NPSL.

Table 1..

@1000 cd m^{-2}	**EQE (%)**	**PE (lm W^{-1})**	**max. ΔCIEx**	**max. ΔCIEy**	**EQEx**
ITO-device	14.07	18.18	0.023	0.022	--
PEDOT-device	12.82	14.85	0.018	0.023	1.00
PEDOT-device with external NPSL	13.98	18.32	0.003	0.001	1.09
PEDOT-device with internal NPSL	17.24	22.14	0.002	0.003	1.34

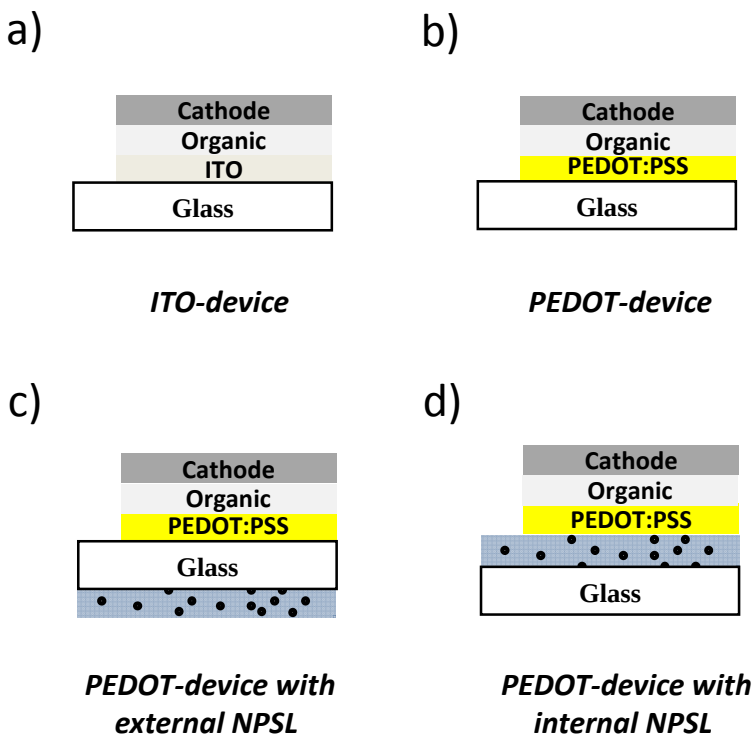
a)
Cathode
Organic
ITO
Glass
ITO-device
b)
Cathode
Organic
PEDOT:PSS
Glass
PEDOT-device
c)
Cathode
Organic
PEDOT:PSS
Glass
PEDOT-device with external NPSL
d)
Cathode
Organic
PEDOT:PSS
Glass
PEDOT-device with internal NPSL

Figure 1.

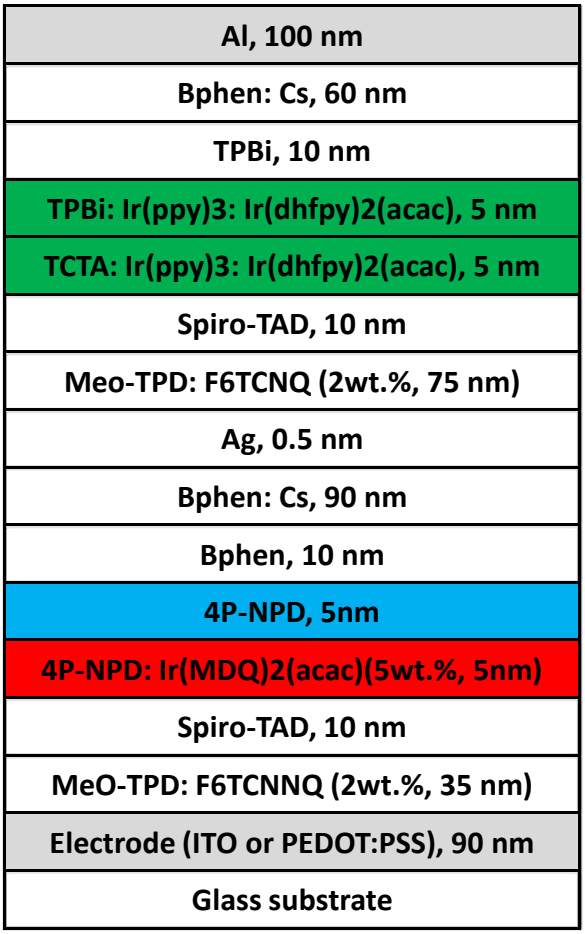
Al, 100 nm
Bphen: Cs, 60 nm
TPBi, 10 nm
TPBi: Ir(ppy)3: Ir(dhfpy)2(acac), 5 nm
TCTA: Ir(ppy)3: Ir(dhfpy)2(acac), 5 nm
Spiro-TAD, 10 nm
Meo-TPD: F6TCNQ (2wt.%, 75 nm)
Ag, 0.5 nm
Bphen: Cs, 90 nm
Bphen, 10 nm
4P-NPD, 5nm
4P-NPD: Ir(MDQ)2(acac)(5wt.%, 5nm)
Spiro-TAD, 10 nm
MeO-TPD: F6TCNNQ (2wt.%, 35 nm)
Electrode (ITO or PEDOT:PSS), 90 nm
Glass substrate

Figure 2.

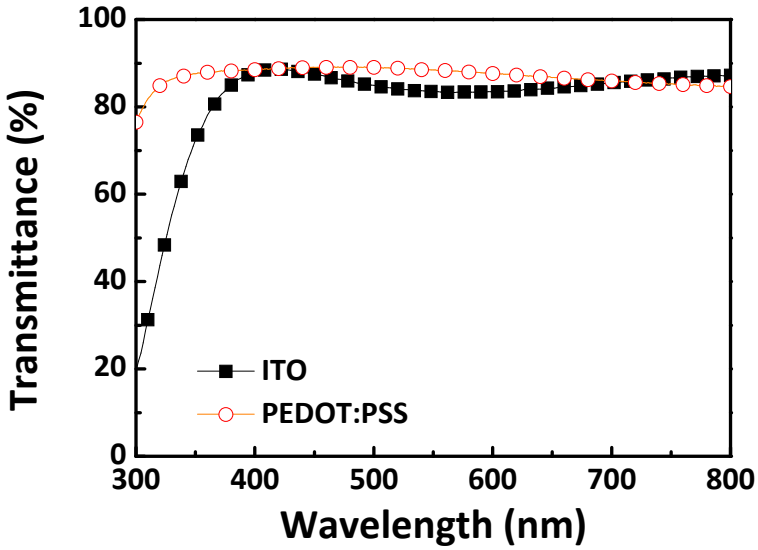
Transmittance (%)
100
80
60
40
20
0
300
400
500
600
700
800
Wavelength (nm)
ITO
PEDOT:PSS

Figure 3.

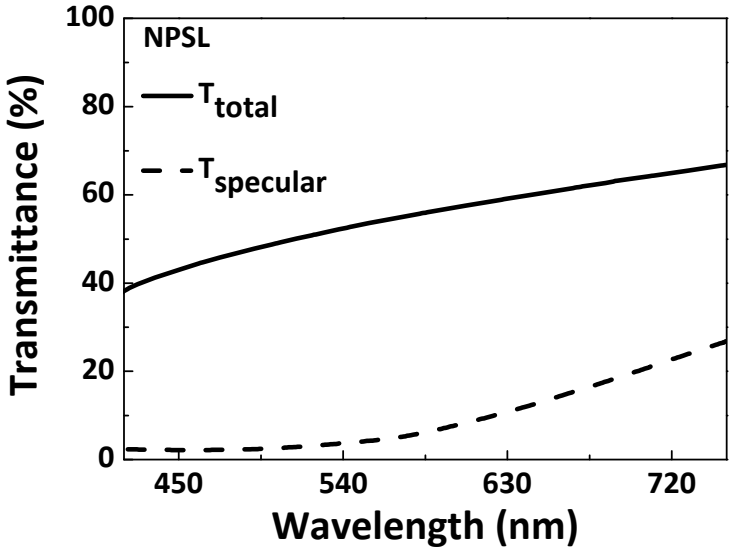
NPSL
T total
T specular
Transmittance (%)
100
80
60
40
20
0
450
540
630
720
Wavelength (nm)

Figure 4.

a)

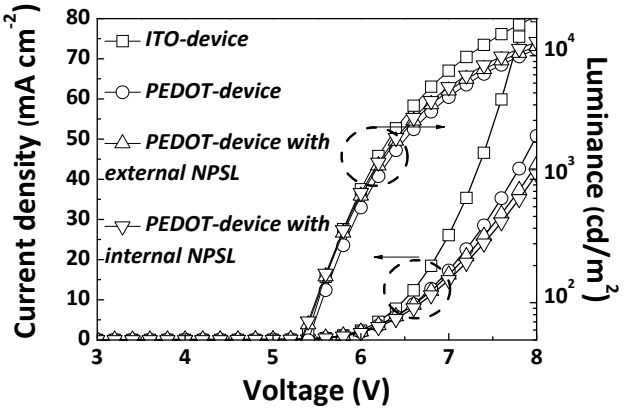
Current density (mA cm^{-2})
Luminance (cd/m^2)
Voltage (V)
ITO-device
PEDOT-device
PEDOT-device with external NPSL
PEDOT-device with internal NPSL

b)

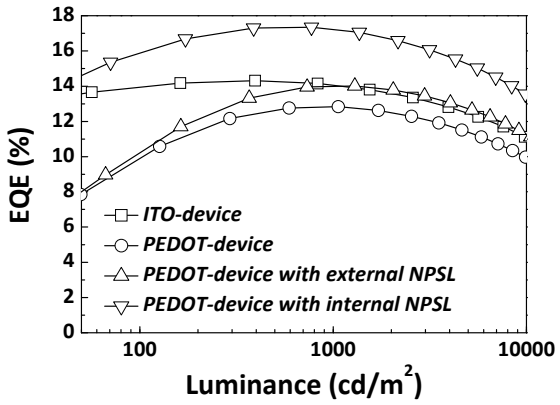
EQE (%)
Luminance (cd/m^2)
ITO-device
PEDOT-device
PEDOT-device with external NPSL
PEDOT-device with internal NPSL

c)

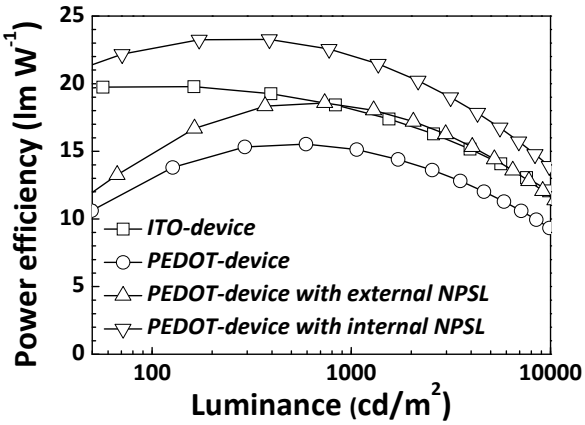
Power efficiency (lm W^{-1})
Luminance (cd/m^2)
ITO-device
PEDOT-device
PEDOT-device with external NPSL
PEDOT-device with internal NPSL

Figure 5.

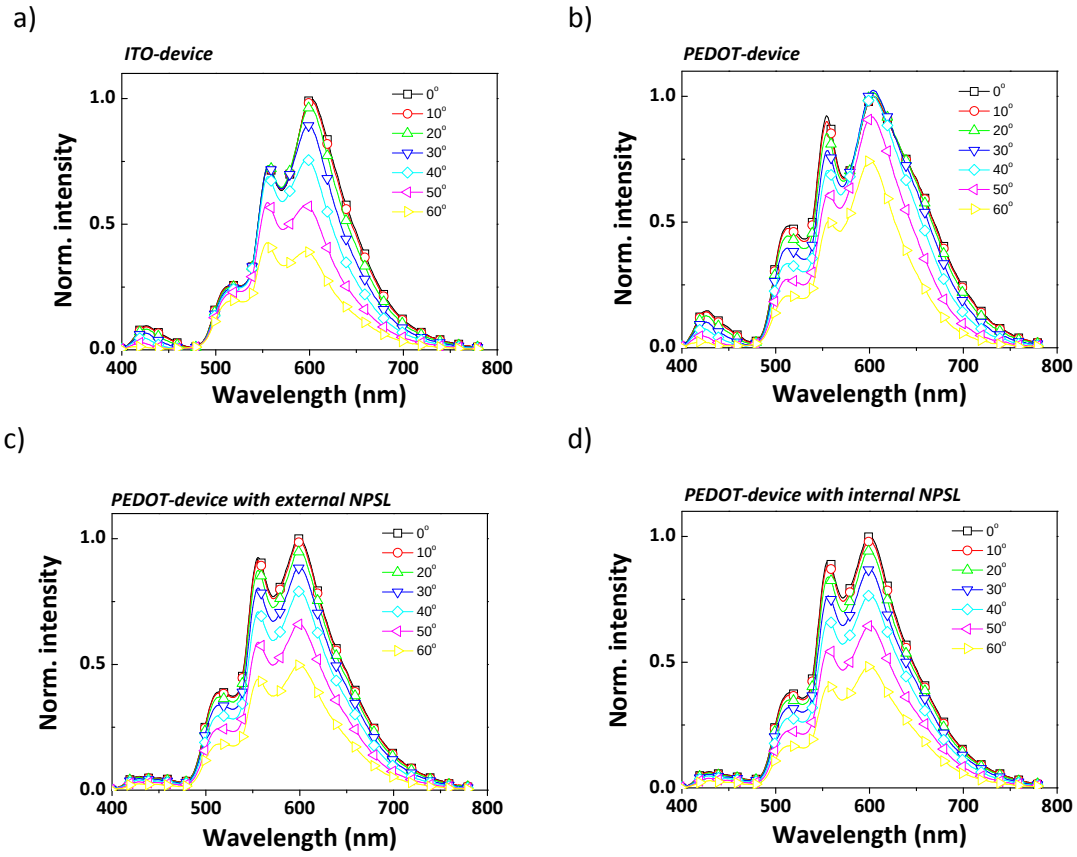
a)
ITO-device
b)
PEDOT-device
c)
PEDOT-device with external NPSL
d)
PEDOT-device with internal NPSL
Norm. intensity
Wavelength (nm)
0°
10°
20°
30°
40°
50°
60°

Figure 6.

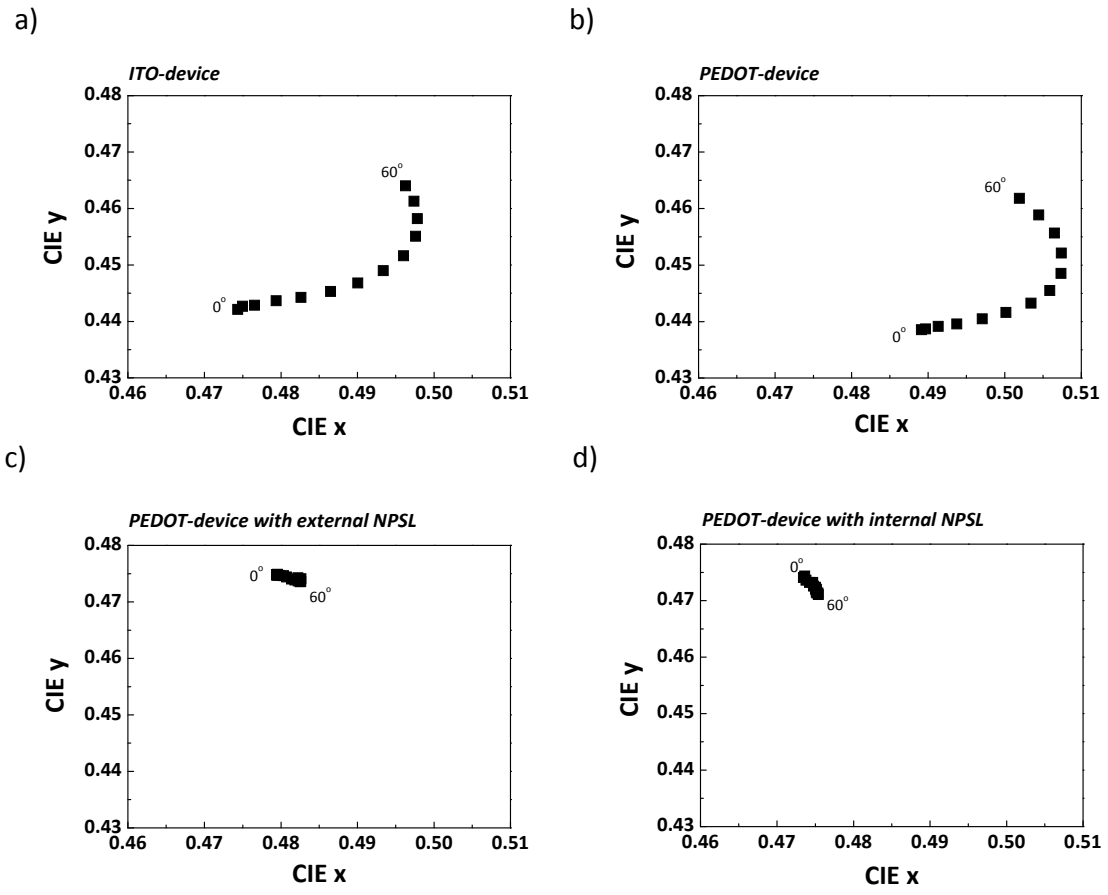
a)
ITO-device
CIE y
CIE x
0.43
0.44
0.45
0.46
0.47
0.48
0.46
0.47
0.48
0.49
0.50
0.51
0°
60°
b)
PEDOT-device
CIE y
CIE x
0°
60°
c)
PEDOT-device with external NPSL
CIE y
CIE x
0°
60°
d)
PEDOT-device with internal NPSL
CIE y
CIE x
0°
60°

Figure 7.